The Abdus Salam
International Centre for Theoretical Physics

United Nations
Educational, Scientific
and Cultural Organization

International Atomic
Energy Agency

SMR 1673/15

AUTUMN COLLEGE ON PLASMA PHYSICS

5 - 30 September 2005

Fluid-Maxwell Simulation of Laser Pulse Dynamics in Overdense Plasma

V. BEREZHIANI

Institute of Physics, Tbilisi, Georgia

Fluid-Maxwell simulation of laser pulse dynamics in overdense plasma

V. I. Berezhiani, D. P. Garuchava, S. V. Mikeladze, K. I. Sigua, and N. L. Tsintsadze
Institute of Physics the Georgian Academy of Science, Tbilisi 380077, Georgia

S. M. Mahajan
Institute for Fusion Studies, University of Texas at Austin, Austin, Texas 78712

Y. Kishimoto
Naka Fusion Research Establishment, JAERI, Naka-Machi, Japan

K. Nishikawa
Faculty of Engineering, Kinki University, Higashi-Hiroshima, Japan

(Received 22 December 2004; accepted 1 April 2005; published online 26 May 2005)

A one-dimensional model of collisionless electron plasma, described by the full system of Maxwell and relativistic hydrodynamic equations, is exploited to study the interaction of relativistic, strong, circularly polarized laser pulses with an overdense plasma. Numerical simulations for the ultrarelativistic pulses demonstrates that for the low as well as for the high background density, the major part of the penetrated energy remains trapped for a long time in a nonstationary layer near the plasma front end; only a minor portion resides in solitons. Important details of the interaction for the moderately intense and strongly relativistic pulses for semi-infinite and thin plasma layers are revealed. An interesting additional consequence of the long-time confinement of relativistic strong radiation in an overdense plasma is analyzed. It is shown that intensive pair production by the driven motion of plasma electrons takes place due to the trident process. © *2005 American Institute of Physics*. [DOI: 10.1063/1.1924708]

I. INTRODUCTION

An exciting era in nonlinear physics has been ushered in by the development of compact terawatt/petawatt laser sources generating subpicosecond pulses of electromagnetic (EM) radiation with focal intensities over $I=10^{20}$ W/cm^2 (Ref. 1) (and the promise of even higher intensity $I=10^{24}$ W/cm^2 pulses[2]). The nonlinear response of an electromagnetically active media could be drastically modified in the intense fields of such pulses. In particular, the strong pulse fields (10^{18} W/cm^2 and higher) will induce relativistic nonlinearities by imparting to an electron an oscillation energy comparable to or even larger than its rest energy. Some expected interesting consequences have already been confirmed by experiments (see, for instance Ref. 2 and references therein).

The dynamics of the penetration of ultraintense laser radiation into overdense plasmas has attracted considerable attention in the past. A few decades ago Kaw and Dawson[3] predicted that the relativistically strong laser radiation can reduce the effective plasma frequency below the self-induced transparency limit (i.e., below the frequency of laser radiation), allowing the laser pulse to penetrate into classically forbidden regions. Interest in this problem was recently renewed (see, for instance, Refs. 4–10) because of two distinct prospective applications: the penetration of intense radiation into an overdense plasma could be crucial in the development of (1) the fast ignitor fusion concept and (2) x-ray lasers.[11] The pulse penetration into the overdense plasma regions becomes possible due to a density modification caused by the ponderomotive pressure of the laser field (as well as the kinetic effects related to the electron heating processes). The most efficient method to investigate the laser-plasma interaction is particle-in-cell (PIC) simulation. However, the simulation results are somewhat difficult to interpret, since the kinetic effects can "shade" and complicate the problem. Although the PIC codes are generally valid over a wide range of regimes, it is desirable to apply a fluid code principally because the PIC models tend to suffer from poor statistical resolution of the motion due to limitations in the number of particles.[12]

The fluid models, though unable to account for trapped particles, wave breaking and other kinetic effects, have the advantage that one has a control over the detailed physics involved. Several aspects of laser pulse dynamics are also easier to establish. Indeed, applying one-dimensional (1D) Maxwell-fluid model, Tushentsov *et al.*[13] charted out two qualitatively different scenarios for the penetration of relativistically intense circularly polarized pulses: (1) For comparatively lower densities (less than $1.5n_c$, n_c is the critical density) penetration occurs through solitonlike structures moving into the plasma and (2) at higher background densities, the laser light penetrates only over a finite length which increases with the incident intensity. In the latter regime the plasma-field structures represent alternating electron layers separated by about half a wavelength of the depleted regions of plasma. Here we note that Bulanov *et al.*,[5] applying PIC simulations, had earlier demonstrated that a part of the energy of the laser pulse can be converted into a localized, relativistically strong, nonlinear electromagnetic pulse propagating into the overdense plasma. However, different regimes of penetration were revealed primarily through the Maxwell-fluid simulations.

Despite its definitive success, the model developed in

Ref. 13 has a serious shortcoming; the Maxwell equations are treated within the framework of a slowly varying envelope (parabolic) approximation. The parabolic approximation clearly breaks down for strongly relativistic intensities when localized solutions consist of a pulse containing a few cycles;[14] it is also invalid in "cavitating" regions where the plasma density tends to vanish. Indeed, in the vacuum region, the electromagnetic field obviously cannot disperse while the paraxial approximation leads to dispersive spreading.

II. BASIC EQUATIONS AND NUMERICAL METHOD

In this paper we abandon the parabolic approximation; we study a collisionless plasma described by the relativistic hydrodynamic equations coupled to the full system of exact Maxwell equations. The electron thermal velocity is assumed to be much smaller than the quiver velocity and the plasma can be treated as a cold electron fluid in a fixed ion background. In this approximation, the Maxwell equations can be written as

$$\nabla \times \mathbf{B} = \frac{1}{c}\frac{\partial \mathbf{E}}{\partial t} - \frac{4\pi e}{c} n \frac{\mathbf{p}}{\gamma m_e}, \tag{1}$$

$$\nabla \times \mathbf{E} = -\frac{1}{c}\frac{\partial \mathbf{B}}{\partial t}, \tag{2}$$

$$\nabla \cdot \mathbf{E} = 4\pi e(n_i - n), \tag{3}$$

where e, m_e, n, and $\mathbf{p}$ are, respectively, the electron charge, mass, density, and momentum, c is the speed of light, $n_i(\mathbf{r})$ is the ion background density, and $\gamma=(1+\mathbf{p}^2/m_e^2c^2)^{1/2}$ is the relativistic factor.

The cold unmagnetized electron fluid obeys the standard relativistic hydrodynamic equations: the equation of motion

$$\frac{\partial \mathbf{p}}{\partial t} + m_e c^2 \nabla \gamma = -e\mathbf{E} \tag{4}$$

and the continuity equation

$$\frac{\partial n}{\partial t} + \nabla \cdot \left(n \frac{\mathbf{p}}{\gamma m_e} \right) = 0. \tag{5}$$

The absence of the magnetic part of the Lorentz force in Eq. (4) is due to the assumption that the generalized vorticity is zero in the body of the electron fluid; this assumption relates the magnetic field with the electron momentum, $\mathbf{B}=(c/e)\nabla \times \mathbf{p}$.[15,16]

It is interesting that Eq. (4) predicts a nonzero plasma momentum for a laser pulse propagating in vacuum. This fact cannot affect the dynamics of the laser pulse in the vacuum region where the plasma density and current are zero ($n=0$). However, a proper modeling of the incident and the reflected laser pulses must demand a self-consistent approach. We recall here that the integration of the relativistic Vlasov equation for a cold plasma leads to the following equation for the momentum density:

$$\frac{\partial n\mathbf{p}}{\partial t} + \nabla : (n\mathbf{v}\mathbf{p}) = -en\left(\mathbf{E} + \frac{1}{c}\mathbf{v} \times \mathbf{B} \right), \tag{6}$$

where $\mathbf{v}=\mathbf{p}/m_e\gamma$. By using the continuity equation (5), Eq. (6) becomes

$$n\left[\frac{\partial \mathbf{p}}{\partial t} + (\mathbf{v}\nabla)\mathbf{p} + e\left(\mathbf{E} + \frac{1}{c}\mathbf{v} \times \mathbf{B} \right) \right] = 0, \tag{7}$$

which, for $n \neq 0$, reduces to the relativistic equation for a cold electron plasma, and which in turn goes over to Eq. (4) in the absence of generalized vorticity. The zero density limit ($n=0$) is degenerate; in this case the fluid equations have no meaning. Shadwick *et al.*[17] argued that the equation of motion in the form of Eq. (6) is fundamental; it is only the currents that have physical significance, for it is the currents that couple the plasma to the electromagnetic fields. We have to bear in mind that the fluid description of the plasmas formally ceases to be valid when $n \to 0$ since the very definition of a fluid implies the presence of a macroscopic number of particles in a unit cell. In this case a kinetic description or PIC simulation is more appropriate than a direct application of Eq. (6). In this paper we ignore kinetic effects; it seems reasonable, therefore, to work with Eq. (4) rather than the more complicated Eq. (6) keeping in mind that the plasma density should never become strictly zero.

In the standard investigations of laser-plasma interactions, a laser pulse impinges on a nonuniform plasma. If the initial density profile is modeled by an analytical function, the plasma density never becomes strictly zero. Thus, far from the dense plasma boundary, i.e., in the "vacuum" region, Eq. (4) can be assumed to be valid implying that the corresponding plasma momentum $\mathbf{p}$ is not zero in this region. The advantage of such an approach is that in the vacuum region the plasma current is negligibly small and the vacuum Maxwell equations can be solved analytically in most cases of interest. Next step is to find the solution of Eq. (4) in a "given" field approximation. These solutions will provide natural initial (boundary) conditions for full set of Maxwell-fluid equations to calculate the subsequent dynamics of the laser pulses in the dense plasma.

It is natural to expect that the approach based on an accurate dynamical treatment of the full set of Maxwell-fluid equations will not lead to the appearance of zero density regions. Our study shows (see below) that under certain conditions a relativistic laser pulse can considerably reduce the electron density in the region of field localization, i.e., electron cavitation can take place. In the cavitating regions the electron density turns out to be a few orders smaller than its original value. However, the density never becomes strictly zero.

For an underdense plasma, the issue of electron cavitation caused by the self-focusing of laser radiation has been discussed in Refs. 18 and 19. The analyses in these studies are based on a quasistatic, paraxial, envelope approximation. While the authors note some of the limitations of the model, they gloss over the biggest limitation—the predictions of negative densities. It is also true that in the model explored in Refs. 18 and 19 [widely used till recent years (see, for instance, Refs. 20 and 21)], the occurrence of nonphysical

negative densities cannot be prevented. This failure of the model is generally corrected by putting $n=0$ in the entire spatial region where $n<0$ (note that in Ref. 22 it is shown that if finite plasma temperature effect is taken into account there will be no singularities in the solution). Qualitative workability of this "operation" is proved in a series of experiments by Borisov *et al.*[23]

It turns out that a similar problem (i.e., appearance of negative densities) plagues the exact 1D analytical stationary solution of the Maxwell-fluid equations. The soliton solution for an arbitrary intense circularly polarized EM radiation for a cold electron plasma is given in Refs. 24–26. It corresponds to a single-hump, nondrifting localized pulse in an overdense plasma. Such a solution exists provided $1<\omega_e^2/\omega^2<1.5$, where $\omega_e=(4\pi e^2 n_0/m_e)^{1/2}$ is the plasma frequency and ω is the soliton frequency; the latter determines the soliton width and the amplitude (see for details Ref. 25) also. With a decrease of ω the field amplitude of the soliton amplitude increases while the corresponding density well deepens. For $\omega_e^2/\omega^2 \geqslant 1.5$ full plasma cavitation is achieved and negative density regions emerge. To combat this problem, Refs. 26 and 27 recommend solving the field equations piecewise, separately in the plasma and the vacuum regions followed by a proper matching at the boundaries. This "surgical" procedure produces consistent density profiles with discontinuous derivatives and spiky spatial gradients. Though such a construction can yield a qualitative understanding of the complex dynamics of laser-plasma interactions; such solutions cannot be realized as exact stationary configurations. Indeed, results of the numerical simulations of Tushentsov *et al.*[13] as well as our studies show that the solutions which resemble the set described above can exist but in a quasistationary fashion. In these solutions, however, a complete cavitation of electrons (electron density going to zero) does not take place.

We will now display the final system for the one-dimensional problem pertinent to a laser pulse normally incident on an overdense plasma (semi-infinite or a finite thickness layer). The Maxwell equations will be written in terms of the vector and scalar potentials, $\mathbf{A}, \phi$. The equilibrium plasma ion density is modeled by the analytical function $n_i(z)=(n_0/2)\,[1+\tanh(z/z_w)]$. The incident laser pulse propagates in the z direction and all dynamical variables are independent of x and y ($\partial_x=\partial_y=0$). The transverse component of the equation of motion (4) is immediately integrated to give $\mathbf{p}_\perp=(e/c)\mathbf{A}_\perp$, where the constant of integration is set equal to zero, since the electron hydrodynamic momentum is assumed to be zero at infinity where the fields vanish.

In terms of dimensionless quantities $n=n/n_0$, $N_w=n_i/n_0$, $\mathbf{r}=(\omega_e/c)\mathbf{r}$, $t=\omega_e t$, $\phi=(e/m_e c^2)\phi$, $\mathbf{A}=(e/m_e c^2)\mathbf{A}$, $\mathbf{E}=(e/m_e\omega_e c^2)\mathbf{E}$, $\mathbf{B}=(e/m_e\omega_e c^2)\mathbf{B}$, and $\mathbf{p}=\mathbf{p}/m_e c$, the governing set of equations in the Coulomb gauge [i.e., $\mathbf{A}=(\mathbf{A}_\perp,0)$] reads

$$\frac{\partial^2 \mathbf{A}_\perp}{\partial t^2}-\frac{\partial^2 \mathbf{A}_\perp}{\partial z^2}+\frac{n}{\gamma}\mathbf{A}_\perp=0, \tag{8}$$

$$\frac{\partial p_z}{\partial t}+\frac{\partial \gamma}{\partial z}=\frac{\partial \phi}{\partial z}, \tag{9}$$

$$\frac{\partial n}{\partial t}+\frac{\partial}{\partial z}\left(\frac{n}{\gamma}p_z\right)=0, \tag{10}$$

$$\frac{\partial^2 \phi}{\partial z^2}=n-N_w(z), \tag{11}$$

where $\gamma=(1+\mathbf{A}_\perp^2+p_z^2)^{1/2}$.

The principal results of this paper are obtained from a numerical integration of Eqs. (8)–(11) for a circularly polarized pulse. For the incident pulse [vacuum solution of Eq. (8)] we choose the form

$$\mathbf{A}_\perp(z,t)=A_0\exp[-0.5(z-z_0-t)^\beta/a_z^\beta]\times\left\{\begin{matrix}\cos[\omega_0(z-z_0-t)]\\ \sin[\omega_0(z-z_0-t)]\end{matrix}\right\}, \tag{12}$$

where A_0 is a measure of the pulse amplitude, a_z is the characteristic width of the Gaussian envelope of the pulse, and ω_0 is the frequency. In dimensional units the pulse amplitude is related to the peak intensity I and the vacuum wavelength ($\lambda_0=2\pi c/\omega_0$) by the relation $I\,(\mathrm{W/cm^2})\lambda_0^2\,(\mu\mathrm{m})=2.74\times10^{18}A_0^2$.[28] Highly relativistic electron motion ($A_0\gtrsim1$) requires, for instance, a laser intensity $I\gtrsim2.74\times10^{18}\ \mathrm{W/cm^2}$ for $\lambda_0=1\ \mu$m.

The initial electron density will be assumed to be equal to the ion density, $n(z,t=0)=N_w(z)$. Note that the solution (12) is valid provided that at $t=0$ the laser field (for any given a_z) is localized sufficiently far from the dense plasma boundary ($z_0\ll0$). In this region the scalar potential vanishes and the solution of Eq. (9) is readily found to be $p_z=\mathbf{A}_\perp^2/2$. Thus at $t=0$ we can provide appropriate initial conditions for the field and the fluid variables; obvious boundary conditions are $Q(\pm\infty,t)=0$ [where $Q\equiv(\mathbf{A}_\perp,\phi,p_z)$], $n(-\infty,t)=0$, and $n(\infty,t)=1$.

To solve the system of equations, a second-order finite difference algorithm has been applied. In the vacuum region the spatial step of the grid is chosen to be 15 times shorter than the vacuum wavelength of the incident pulse. Interaction of the strong laser field with the plasma leads to the development of areas with sharp density gradients. Consequently, in these regions, the spatial steps are further reduced to 1/10 of their values in the vacuum region. The spatial computational window is dynamical, i.e., the boundaries of the window move out faster than any perturbation of the fields. The temporal step is dictated by the stability criterion of the scheme. Thus, both the spatial and the temporal steps of the grid are variable. The wave equation (8) was approximated by an implicit second-order discrete equation and solved by the modified Gauss method. For Eqs. (9) and (10) the first-order, explicit scheme was applied. In this scheme the spatial derivatives are approximated by "left" differences. To prevent density overshooting, the Lax scheme was applied. However, a direct application of the standard Lax method **(**where temporal derivatives are approximated by $[f_j^{k+1}-0.5(f_{j-1}^k+f_{j+1}^k)]/\tau_k$**)** leads to the development of ripples at the base of the density pedestal. In our scheme the temporal derivatives are discretized by $\{f_j^{k+1}-0.5(h_j+h_{j-1})^{-1}[h_j f_{j-1}^k+(h_j+h_{j-1})f_j^k+h_{j-1}f_{j+1}^k]\}/\tau_k$. Here h_j and τ_k are, respectively, the spatial and the temporal steps of the

grid. This modification of the Lax method prevents occurrence of the ripples. The accuracy of the numerical scheme was controlled by the integrals of motion. We ensure the conservations of the energy

$$\varepsilon = \frac{1}{2}\int dz\left[\left(\frac{\partial \mathbf{A}_\perp}{\partial t}\right)^2 + \left(\frac{\partial \mathbf{A}_\perp}{\partial z}\right)^2 + \left(\frac{\partial \phi}{\partial z}\right)^2 + 2n(\gamma - 1)\right] \tag{13}$$

and the total momentum

$$\mathcal{P}_z = \int dz p_z, \tag{14}$$

and demand charge neutrality (at each step)

$$\mathcal{Q} = \int dz[n - N_w(z)] = 0. \tag{15}$$

Boundaries of the integrals are taken beyond the areas of field localization where all fluxes are zero.

It is worthwhile to state that in our algorithm most of the problems related to the 1D Maxwell-fluid simulations described in Ref. 17 are overcome for circularly polarized pulses. In particular, the appearance of negative density areas, ripples, and density overshoots at the vacuum-plasma interface are prevented. Our numerical algorithm can also be used to study certain aspects of the dynamics of linearly polarized pulses, of pulses containing just a few optical cycles of radiation, and for harmonic generation and Raman scattering processes. However, for linearly polarized pulses impinging on the sharp boundary of overdense plasma a kinetic effect known as "electron vacuum heating" at the plasma-vacuum interface[29] can lead to a significant absorption of the laser pulse energy; this effect is outside the domain of the Maxwell-fluid model. This absorption mechanism is related to the oscillating component of the ponderomotive force which drives electrons across the vacuum-plasma interface. The ponderomotive force of the circularly polarized pulses, however, contains no oscillating component; the vacuum heating of the electrons, therefore, is not expected to significantly alter the results obtained by the Maxwell-fluid approach.

III. NUMERICAL SIMULATIONS: OVERDENSE PLASMAS

A. Weakly relativistic pulses

In order to benchmark the numerical code developed and used for this paper, we first verify a well-known exact analytical soliton solution of Eqs. (8)–(11). For a uniform ion density ($N_w=1$), the soliton solution is found to be[25]

$$\mathbf{A}_\perp = [\cos(\omega t), \sin(\omega t)]\frac{2\sqrt{1-\omega^2}\cosh(\sqrt{1-\omega^2}z)}{\cosh^2(\sqrt{1-\omega^2}z) + \omega^2 - 1}, \tag{16}$$

with amplitude $A_0 = 2\sqrt{1-\omega^2}/\omega^2$ and a characteristic width $l \approx 1/\sqrt{1-\omega^2}$.

Taking into account that $p_z=0$ and $\phi=\gamma-1$, the electron density distribution can be computed from $n=1+\partial^2\gamma/\partial z^2$. The minimum value of the electron density achieved is at the center of solitary structure, $n(0)=1-4(1-\omega^2)^2/\omega^4$. At $\omega=(2/3)^{1/2}$ when the soliton amplitude is $A_{0m}=3^{1/2}$ the electrons are expelled completely from the center $[n(0)=0]$. For $A_0>3^{1/2}$ $[\omega<(2/3)^{1/2}]$ the solution contains a region where the electron density is negative which implies that wave breaking takes place. Thus, in a cold electron plasma the stationary circularly polarized soliton solution exists provided $(2/3)^{1/2}<\omega<1$ while its amplitude cannot exceed $A_{0m}=3^{1/2}$. Our numerical simulations demonstrate exceptional stability of the solution (16); this is in full agreement with the results obtained by PIC simulations in Ref. 25 (see Fig. 1). For $A_0=1.5$ and $\omega=0.84$ (the case considered in Ref. 25) the soliton indeed preserves its shape and amplitude for a long time.

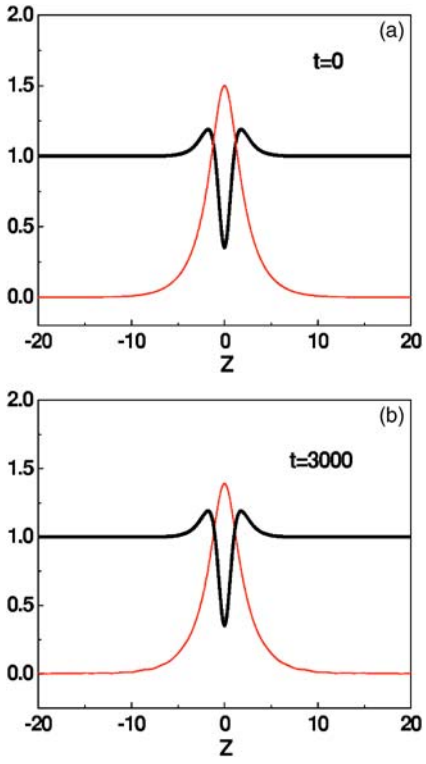

FIG. 1. Stability of the soliton of amplitude $A_0=1.5$ given by Eq. (16). The transverse field $|\mathbf{A}_\perp|$ (thin, red line) and plasma electron density n (thick, black line) spatial profiles are shown at $t=0$ and $t=3000$.

Next we study the problem of pulse penetration in an overdense semi-infinite plasma in conditions similar to those presented in Ref. 13. The parameters of incident laser pulse (12) at $t=0$ are taken to be $A_0=0.71$, $a_z=114$, $\beta=4$, $z_0=-300$. The frequency of radiation is $\omega_0=0.88$; it corresponds to $n_0=1.3n_{cr}$ where $n_{cr}=(m_e\omega_0^2/4\pi e^2)$ is the critical density. For radiation with $\lambda_0=1$ μm the critical density is calculated to be $n_{cr}=1.1\times10^{21}$ cm^{-3}. In physical units, these parameters imply the following: the laser intensity $I\simeq1.38\times10^{18}$ W/cm^2, the pulse duration (full width at half maximum) $T_p\simeq100$ fs, and the longitudinal width $L_p\simeq30$ μm. To better appreciate the results of forthcoming simulations we remark that 100 units of dimensionless t and z correspond, respectively, to 47 fs temporal and 12 μm spatial intervals.

In Fig. 2 the spatiotemporal dynamics of the process is

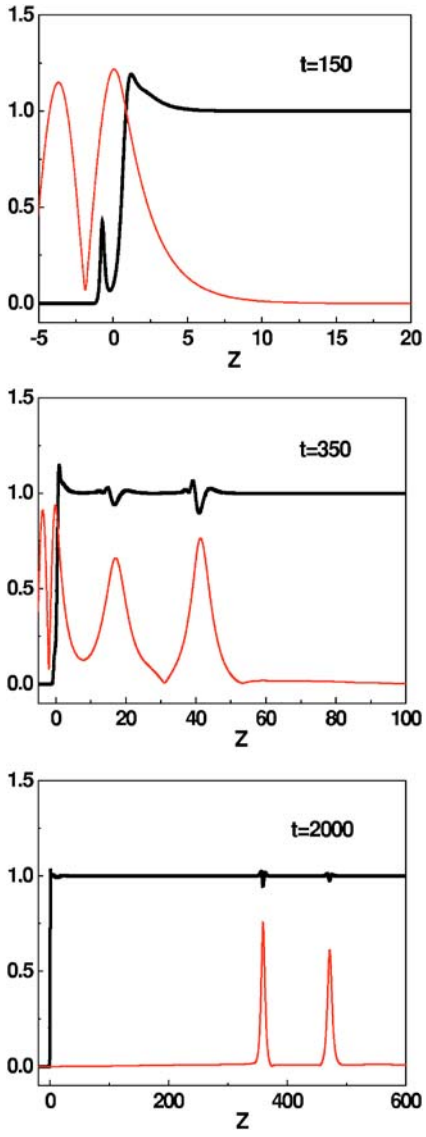

FIG. 2. Snapshots of the time evolution of the electron density (thick, black line) and the transverse field $|\mathbf{A}_\perp|$ (thin, red line) for the incident laser pulse with $A_0=0.71$, $a_z=114$, and $\omega_0=0.88$ impinging on the semi-infinite plasma with sharp density slope $z_w=0.3$.

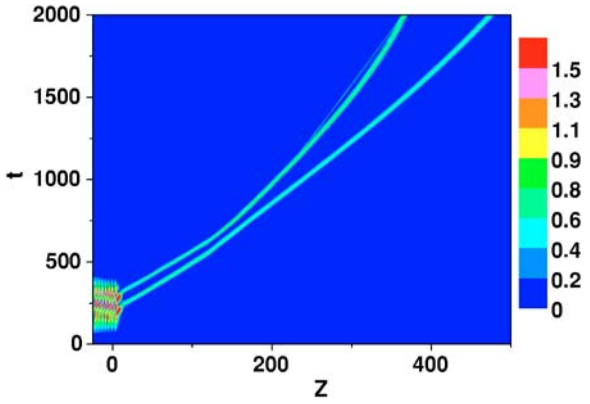

FIG. 3. The t-z diagram of $|\mathbf{A}_\perp|$ for conditions pertaining to Fig. 2.

demonstrated when there exists a sharp density slope at the plasma boundary. The characteristic width of the slope is $z_w=0.04\lambda_0=0.3$, where $\lambda_0\approx 7$ is the dimensionless vacuum wavelength of radiation. One can see that in agreement with the results of Ref. 13, two solitary single-humped waves are generated at the plasma boundary and then they slowly propagate as quasistationary plasma-field structures. These two slightly overlapping solitons near the plasma boundary are moving with almost the same velocity $v\approx 0.33c$. As one can better see in the contour plot (see Fig. 3) these structures eventually decelerate and decouple. The velocity of the leading but lower amplitude soliton tends to $v\approx 0.2$ while the trailing soliton settles to a velocity $v\approx 0.11$. Considerable part of the pulse is reflected carrying up to 90% of the energy in the incident pulse. The spectrum of the reflected radiation is mostly redshifted. This is related to the Doppler shift due to the motion of the vacuum-plasma boundary. Indeed, in the early, transient stage of interaction (when the bulk is reflected back) the plasma electrons are pushed in the direction of the incident pulse propagation. Thus reflection occurs from a moving plasma mirror resulting in redshifting of the reflected pulse.

On a slight change of the characteristic width of the initial density slope ($z_w=0.5$), keeping all other parameters unaltered, the dynamics of pulse propagation changes markedly (as seen in Fig. 4). After the transient stage of interaction three single-humped solitary waves are, now, generated. The leading soliton (similar to the one in the preceding example) has a weakly relativistic amplitude $A_{m1}\approx 0.44$ and propagates with a constant velocity $v_1=0.26$. In the contour plot (Fig. 5) the straight line corresponds to this soliton. The spectrum of the soliton field ($\sim|A_y(\omega)|^2$), displayed in Fig. 6, is blueshifted and its intensity reaches a maximum value at $\omega_1=1.17\omega_0=1.0296$. The analytical solution obtained in Refs. 30 and 31 in the limit of weak density response [see Eqs. (8) and (9) in Ref. 31] describes this soliton profile quite well. The carrier frequency of the soliton may be found from the relation

$$\omega_1=\frac{[16(1-v_1^2)^2+A_{m1}^2(1-v_1^2)(3+v_1^2)]^{1/2}}{(1-v_1^2)[4A_m^2+16(1-v_1^2)]^{1/2}}. \tag{17}$$

For $A_{m1}=0.44$ and $v_1=0.26$, Eq. (17) gives $\omega_1=1.0296$ which is in agreement with the numerical result.

The weakly relativistic soliton described above is followed by two moderately relativistic solitary pulses with $A_{m2}=1.07$ and $A_{m3}=0.97$, which are formed near the plasma boundary. After initial deceleration they acquire small velocities; At $t=2000$ the velocities of the second (third) soliton tend to $v_2=0.005$ ($v_3=0.015$) as shown in Figs. 4 and 5. The field and the density shape are well approximated by the exact analytical solution given by Eq. (16). The spectral analysis shows that envelopes of these single-hump solitons oscillate with frequencies below the unperturbed plasma frequency: $\omega_2=0.89$ and $\omega_3=0.95$. Note that in Fig. 4 we plot the evolution of $|\mathbf{A}_\perp|$ and consequently these oscillations cannot be seen (the oscillations could be observed if we were to plot the evolution of A_x or A_y—the components of the vector potential). Knowing the frequencies of oscillations one can calculate, using Eq. (16), the corresponding ampli-

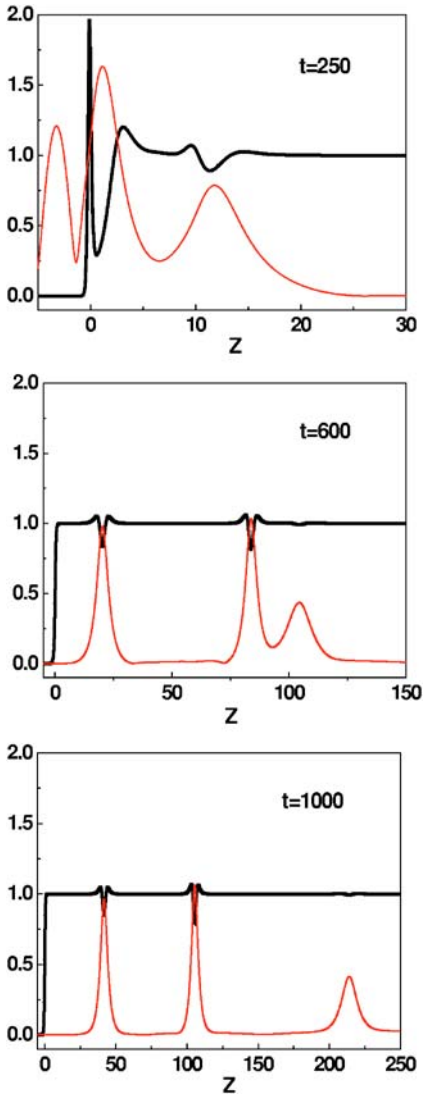

FIG. 4. Snapshots of the time evolution of the electron density (thick, black line) and the transverse field $|\mathbf{A}_\perp|$ (thin, red line) when the characteristic width of the initial density slope is $z_w=0.5$—other parameters are the same as in Figs. 2 and 3.

tudes of the solitons. These amplitudes are $A_{m2}=1.09$ and $A_{m3}=0.96$—very close to the results obtained by numerical simulations.

The reflected part of radiation is redshifted and carries up to 85% of the incident energy. The remaining 15% of the

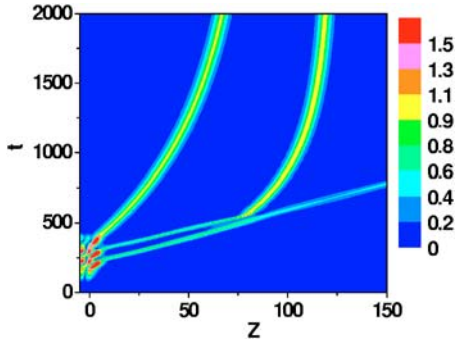

FIG. 5. The t-z diagram of $|\mathbf{A}_\perp|$ for conditions as in Fig. 4.

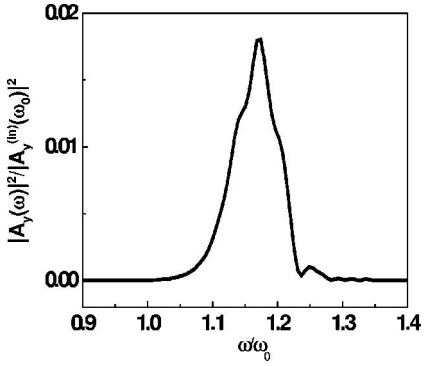

FIG. 6. The spectral intensity of the soliton field ($|A_y(\omega)|^2$) normalized to maximal spectral intensity of the incident pulse $|A_y^{(\mathrm{in})}(\omega_0)|^2$ vs ω/ω_0.

energy penetrates into the overdense region in two distinct but related forms: weakly relativistic, slowly moving solitons (with a weak density response), and moderately relativistic solitons with even smaller velocities but with a considerable density response. Frequencies of the solitons are blueshifted in comparison to the vacuum frequency of the incident pulse [note, however, the frequencies of the very slow solitons remain below the equilibrium Langmuir frequency ($\omega_{2,3}<1$)]. The blueshifting takes place at the vacuum plasma boundary (where the pulse encounters a rapid increase in the electron density) as a result of the ponderomotive pressure.[32]

The semi-infinite plasma is a model—What happens when the laser pulse impinges on a plasma of finite thickness? In the cases described above, the pulse enters the plasma and assumes solitonic behavior in about 50–100 clas-

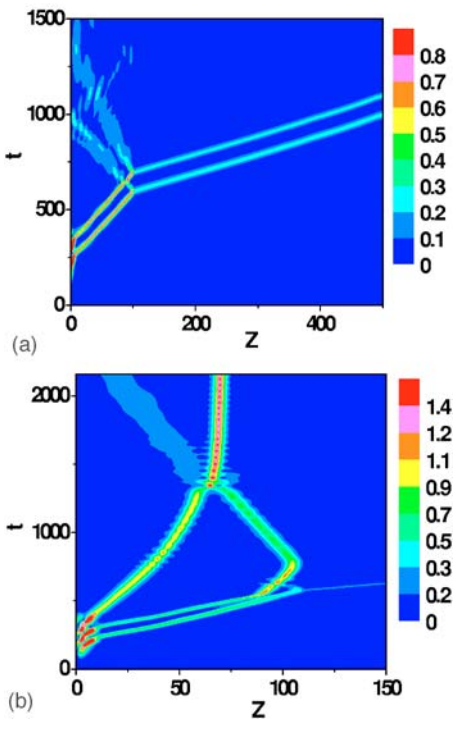

FIG. 7. The t-z diagram of $|\mathbf{A}_\perp|$ describing the dynamics of solitons in the layer (a) corresponding to the parameters of Fig. 3 and (b) corresponding to Fig. 5.

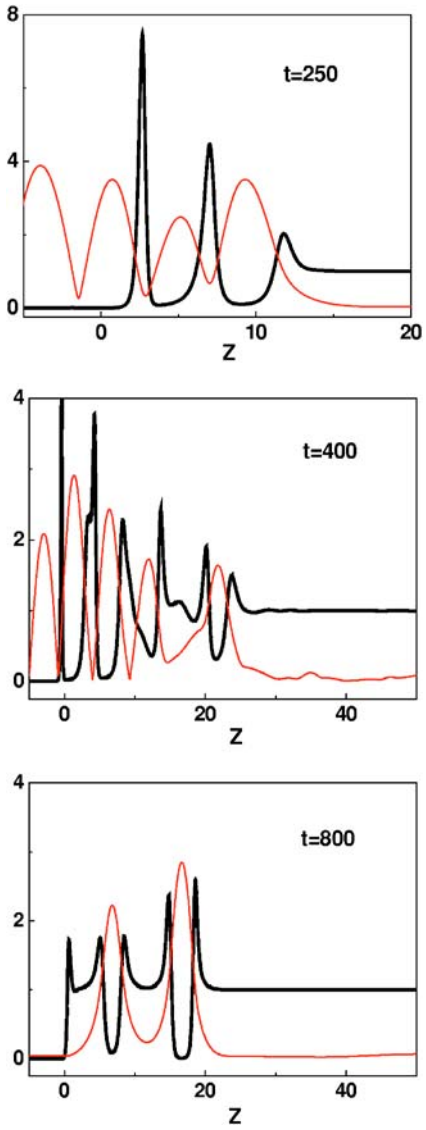

FIG. 8. Snapshots of the time evolution of the electron density (thick, black line) and the transverse field $|\mathbf{A}_\perp|$ (thin, red line) for the incident pulse with $A_0=1.9$, $a_z=126$, and $\omega_0=0.8$ impinging on the semi-infinite plasma with sharp density slope $z_w=0.3$.

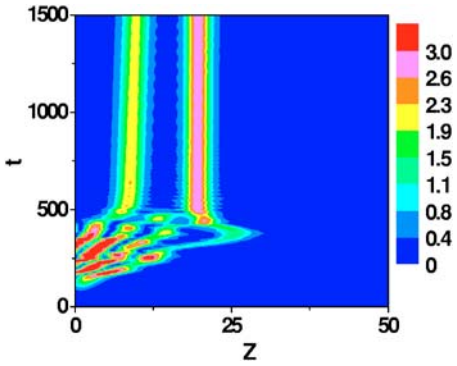

FIG. 9. The t-z diagram of $|\mathbf{A}_\perp|$ for the conditions of Fig. 8.

sical skin depths ($=c/\omega_e$). It is natural to expect that if the thickness of the plasma layer is larger than the soliton-formation distance, these slowly moving solitons eventually reach the plasma end and leave it in the form of an EM pulse sequence. We examine the penetration of the pulse through a plasma layer of thickness $L=100$ for the same values of the parameters as in Figs. 3 and 5. In Fig. 7(a), the contour plot shows the soliton dynamics in the layer for the parameters of Fig. 3. The solitons leave the plasma layer in the form of two EM pulses while the reflected (from the frontier) energy is small. In Fig. 7(b), corresponding to the parameters of Fig. 5, one can see that the leading soliton leaves the layer in the form of a single EM pulse carrying just 3% of the energy of the incident pulse. The following larger amplitude (and slower moving) soliton is reflected from the frontier and merges with the third soliton. Subsequently, just one solitary structure is formed and remains in the layer with almost zero velocity. The energy of the radiation which is locked in the plasma layer is 12% of energy of incident pulse.

Thus the full fluid-Maxwell code verifies that for $n_0 < 1.5n_{cr}$, the moderately intense laser pulses penetrate into the overdense plasma region in the form of solitons as predicted (Ref. 13). The details of soliton formation and the number, amplitude, shape, and other characteristics of the generated solitons, however, are quite sensitive to initial conditions. These details could lead to different scenarios of pulse dynamics in a thin plasma layer. The generated solitons may not, in fact, leave the plasma but can be locked in the layer keeping a considerable part of energy of the incident pulse.

Now we turn our attention to higher background densities, $n_0 > 1.5n_{cr}$. According to Ref. 13, for these high densities, the interaction of the laser pulse with a semi-infinite electron plasma might result in the generation of a plasma-field structure consisting of alternating electron and vacuum regions, with the electromagnetic energy penetrating into the overdense plasma over a finite length determined by the incident intensity. To better compare our findings with Ref. 13, we performed our numerical simulations for the parameters used in this reference. The vacuum amplitude and the width of the pulse are taken to be, respectively, $A_0=1.9$ and $a_z=126$. The plasma density $n_0=1.6n_{cr}$ corresponds to the laser field frequency $\omega_0=0.8$. For radiation with $\lambda_0=1$ μm, the pulse intensity is $I\approx 10^{19}$ W/cm^2 while the pulse duration ($T_p\simeq 100$ fs) and the spatial longitudinal width ($L_p \simeq 30$ μm) are the same as in the previous cases (Figs. 2–7). We remind the reader that 100 units of t and z correspond to 42 fs and 13 μm, respectively.

In Fig. 8 we display the interaction dynamics when the density slope is sharp, $z_w=0.3$. One can see that, in agreement with the results of Ref. 13, in the first stage of interaction a part of the pulse penetrates into the plasma over a fixed finite length creating deep density cavities, while a considerable part of the EM energy is reflected. Localized near the plasma boundary, the field-density structure exhibits highly nonstationary behavior. In the next stage (after the laser drive has vanished), the energy localized inside the plasma is reflected back towards the vacuum, leaving in the plasma just two localized deep density cavities. The pulses are trapped in these, almost motionless quasistationary cavities (see contour plot in Fig. 9). Results corresponding to the

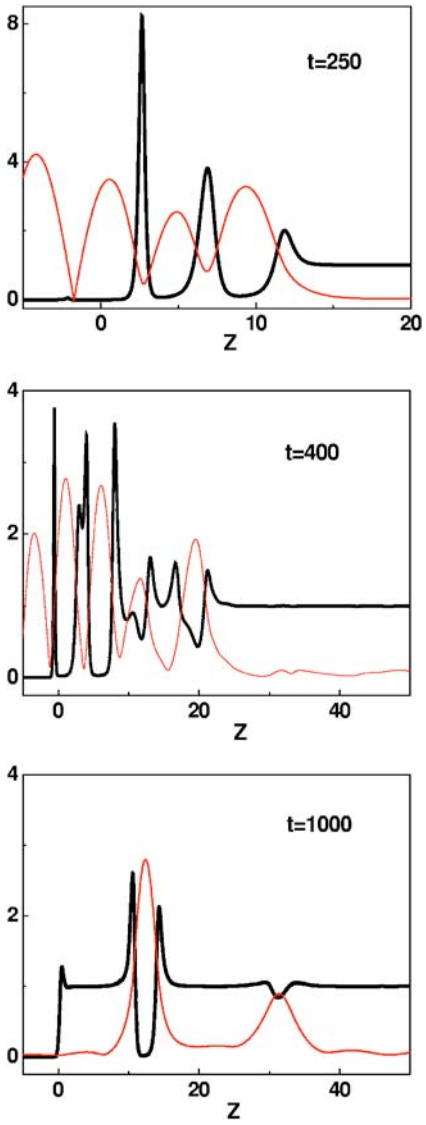

FIG. 10. Snapshots of the time evolution of the electron density (thick, black line) and the transverse field $|\mathbf{A}_\perp|$ (thin, red line) when the characteristic width of the initial density slope is $z_w=0.5$—other parameters are the same as in Figs. 8 and 9.

same conditions as in Fig. 8, but with a slightly increased density slope $z_w=0.5$, are presented in Figs. 10 and 11. One can see that this slight increase causes a major change—we are now left with a single density cavity near the plasma boundary, we also see the emergence of a slowly moving soliton. The soliton has a velocity $v=0.03$, $A_m=0.8$ with a blueshifted mean frequency $\omega=0.92$. The shape and the parameters of the soliton are well described by Eq. (16). The reflected part of the radiation is mostly redshifted and carries up to 90% of the incident energy. Main part of the penetrated energy is trapped in the deep density cavity while just 2% of the energy resides in the slowly moving soliton. In case of a thin plasma layer, for instance, with thickness $L=50\approx 6\lambda_0$, the soliton leaves the layer at $t=1500$; the same distance in the vacuum will be traversed by the pulse in $t=320$ (note that at $t=0$ the incident pulse is "situated" at $z_0=-280$). This example and the other cases considered earlier (see Fig. 7) demonstrate that an overdense plasma layer can be a very

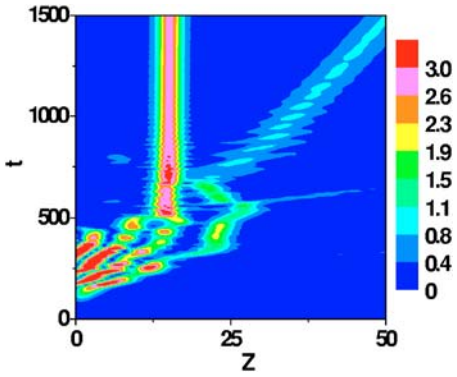

FIG. 11. The t-z diagram of $|\mathbf{A}_\perp|$ for the conditions of Fig. 10.

effective instrument for "slowing" light down, and can be used for the plasma based signal processing for strong laser radiation. Note that in Nonlinear Optics, different schemes for lowering the speed of weak intensity laser radiation are being actively investigated (see, for instance Refs. 33 and 34).

We would like to emphasize that during the entire period of interaction, the electron density never becomes zero. In simulations presented above, the density in the depleted regions never dropped below $n_{\min}\approx 0.01 n_0$. Integrals of motion were conserved with a good precision, for instance, the energy integral ε was conserved with 1% accuracy while accuracy of the momentum integral conservation $\mathcal{P}_z$ and the total charge $\mathcal{Q}$ conservation was much better.

Thus, simulations of exact 1D Maxwell-fluid equations not only confirm qualitatively the results obtained in Ref. 13 for moderately intense laser pulses, but also reveal quantitative difference as well as reveal important features of the interaction.

At the end of this section we would like to emphasize that penetration of the laser pulse into overdense regions in the form of solitons is not the only possible scenario. Let us, for instance, consider an ultrashort incident pulse of a few optical cycles. The frequency spectrum of such a pulse is rather broad implying that even if the carrier frequency $\omega_0<1$, some part of the spectral energy will lie in the region $\omega>1$. For the high frequency part of the radiation, therefore, the "overdense" plasma does not remain overdense, and the penetration takes place without the aid of relativity or of nonlinear effects. We illustrate this by studying the case of a semi-infinite slab with a sharp boundary ($z_w=0.5$), a time independent electron density $n=N_w(z)$, and nonrelativistic electrons (and $\gamma=1$). The incident super-Gaussian ($\beta=4$) laser pulse has the following characteristics: the amplitude $A_0=0.71$, the frequency $\omega_0=0.88$, and $a_z=8$; the pulse is composed of only four cycles. In Fig. 12(a) we present the frequency spectra of the incident and the reflected radiations. The spectra of the reflected and the incident radiations are found to coincide except in the cutoff part of spectrum with $\omega>1$. The related part of energy penetrates the plasma in the form of a classical linear dispersive wave pulse peculiar to an underdense plasma [see Fig. 12(b)]. The underdense electron plasma case is beyond the intended scope of the current paper and will not be pursued further.

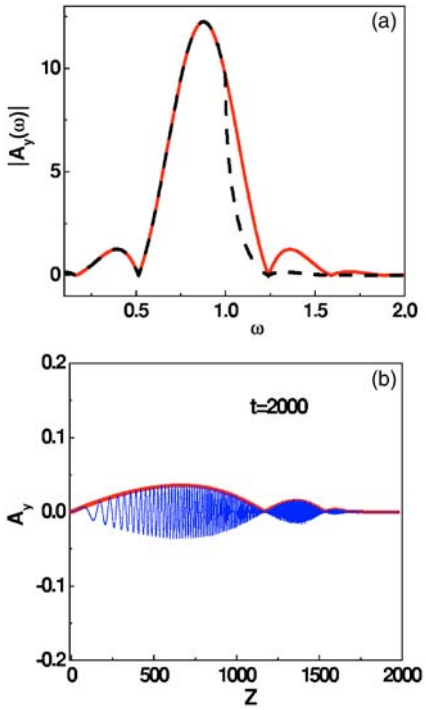

FIG. 12. (a) The frequency spectra of incident (solid line) and reflected (dashed line) radiation for the ultrashort pulse: $A_0=0.71$, $\omega_0=0.88$, and $a_z=8$. (b) The profile of the penetrated (in plasma) laser field A_y vs z at $t=2000$.

B. Ultrarelativistic pulses

The following is the main question we would like to address now: Do the ultrarelativistic laser pulses penetrate overdense plasmas as the moderately relativistic pulses do or is the penetration dynamics distinctly different? We seek the answer by raising the pulse amplitude to the range $A_0^2 \gg 1$ in our simulations. We will deal with densities both less and greater than 1.5 times the critical density. We saw in the previous sections that for lower densities, the penetration of moderately intense pulses occurs by solitonlike structures moving into the plasma.[13] However, it seems reasonable to expect that soliton generation as the main mechanism of energy penetration for ultrarelativistic pulses may not hold. There are following arguments supporting such a conclusion. First, in PIC simulations[4–10] conducted earlier (mostly for ultrarelativistic pulses) the intensive generation of solitons was not observed at the vacuum boundary of an overdense plasma. Second, the known stable solitonic structures do not have ultrarelativistic amplitudes {for instance, the amplitude of the slowly moving relativistic solitons cannot exceed the value $A_{0m}=3^{1/2}$ [see Eq. (16)]}. The solitonic mode may not be the principal mode for penetration even if the dynamics may have an inherent tendency to force an eventual arrangement of the penetrated energy into solitons; the time scales needed for the solitonic mode to emerge could be far in excess of the ion motion time or the dissipation time for the ultrarelativistic incident pulses.

Our numerical simulations for ultraintense pulses show that in both the density regimes [the low ($n_0<1.5n_{cr}$) and the high ($n_0>1.5$)], the bulk of the penetrated energy is trapped in a nonstationary layer near the plasma boundary; the trapping persists for a long time. To demonstrate the essential details of the process, we present the results of the numerical simulations for an ultrarelativistic pulse with $A_0=5$ in Figs. 13 and 14. For the simulation resulting in Fig. 13, the frequency of the incident pulse is $\omega_0=0.88$ (i.e., $n_0=1.3n_{cr}$) and the pulse width is $a_z=114$, while for Fig. 14, the corresponding numbers are $\omega_0=0.8$ ($n_0=1.6n_{cr}$) and $a_z=126$. We choose $t=0$ to be the instant when the peak of the super-Gaussian ($\beta=4$) envelope is situated in the vacuum region at $z_0=-300$. The characteristic width of the slope of the semi-infinite plasma is assumed to be sharp, $z_w=0.3$. For $\lambda_0=1$ μm the corresponding peak intensity and the pulse duration are, respectively, $I\simeq 6.85\times 10^{19}$ W/cm^2 and $T_p\simeq 100$ fs.

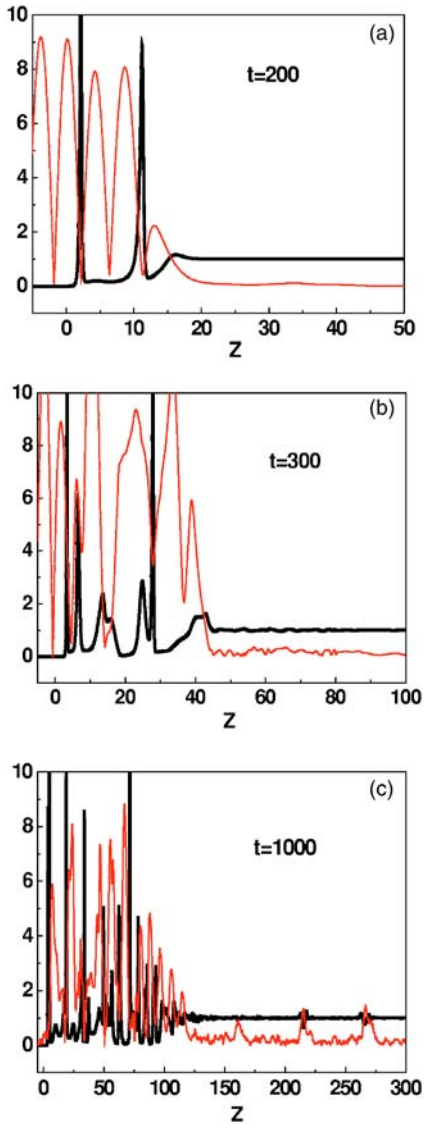

FIG. 13. Snapshots of the time evolution of the electron density (thick, black line) and the transverse field $|\mathbf{A}_\perp|$ (thin, red line) for the incident laser pulse with $A_0=5$, $a_z=114$, and $\omega_0=0.88$.

Evidently, the penetration dynamics for the two cases have similar features (Figs. 13 and 14). The high-frequency pressure of the laser field induces considerable modification of the plasma density profile near the vacuum-plasma bound-

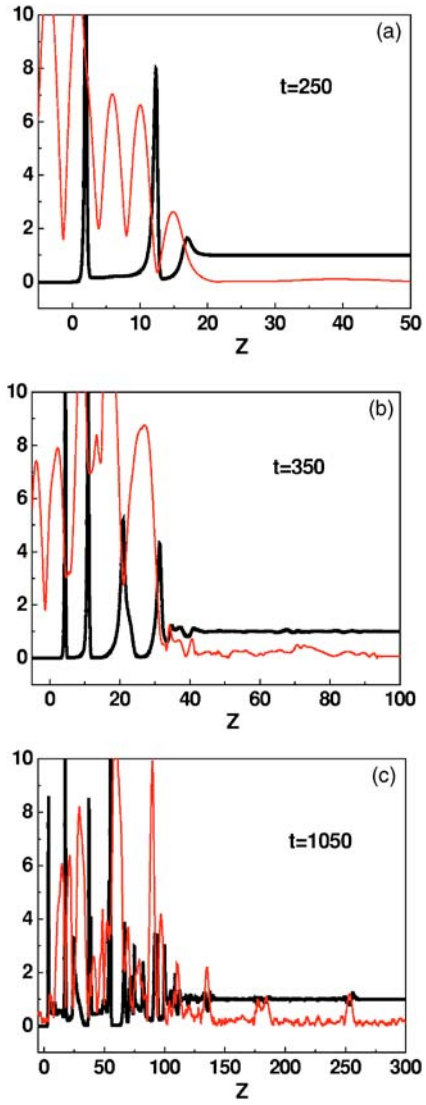

FIG. 14. Snapshots of the time evolution of the electron density (thick, black line) and the transverse field $|\mathbf{A}_\perp|$ (thin, red line) for the incident laser pulse with $A_0=5$, $a_z=126$, and $\omega_0=0.8$.

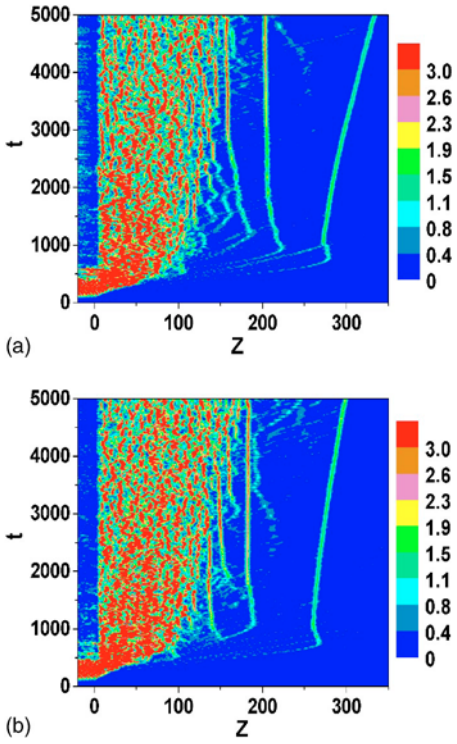

FIG. 15. (a) and (b) the t-z diagram of $|\mathbf{A}_\perp|$ in the same conditions as given in Figs. 13 and 14, respectively.

ary. In the early stages of the interaction, the laser pulse, pushing plasma electrons into the plasma interior, creates a strongly overcritical but a thin plasma "wall." Part of the pulse energy is reflected back, while a part pushes its way past the first wall and begins creating (in front of it) another plasma wall. This process goes on till the energy penetrates to a certain depth ($z\approx 150$). The plasma electron distribution consists of a sequence of overcritical density spikes separated by deep density wells where parts of the EM radiation are trapped. This structure is highly nonstationary allowing leakage of the trapped radiation in both the front and the backward directions. In Figs. 13(c) and 14(c) one can see that in regions deep into the plasma, the solitonic structures form in both the cases. The amplitudes of these solitons are rather small; the bulk of the penetrated energy still resides near the plasma boundary and is not carried by solitons. We conducted simulations for a long time ($t=5000$) to check if any intensive generation of solitons occurs at subsequent stages of the system evolution (notice that for laser pulse with $\lambda_0=1$ μm this time exceeds 2 ps).

In Figs. 15(a) and 15(b) the results of the long-time simulations are presented in the form of contour plots. We find that, in both the cases, the bulk of the penetrated (in plasma) energy remains locked near the plasma boundary during the entire spell ($0<t<5000$) although a few solitons are generated in both the cases. For the lower density plasma [Fig. 15(a)], up to 14% of the incident energy is locked in the region $0<z<150$, and just 2.6% of the energy is stored into solitons and quasiperiodic low amplitude train of waves beyond $z>150$. For the higher density case [Fig. 15(b)], the corresponding numbers are 11% and 2.7%. Thus, we can conclude that for ultrarelativistic pulses, the difference in penetration between the two density regimes essentially disappears; there is no critical density like the one that exists for moderate amplitude pulses. In both the cases the bulk of the penetrated energy resides at the vacuum plasma boundary; solitonlike structures are formed but they account for a rather minor part of the energy. Frequencies of the solitons are blueshifted in comparison to the vacuum frequency of the incident pulse.

The main part of the incident pulse energy (up to 85%) is reflected back from the nonsteady plasma configuration at the vacuum boundary. The profile of the reflected radiation at $t=5000$ for the high density case ($\omega_0=0.8$) is presented in Fig. 16(a) (similar behavior pertains for low density case). The reflected signal consists of a highly modulated pulse followed by a long train of short subpulses. The spectrum of the reflected field is basically redshifted [see Fig. 16(b)]. A

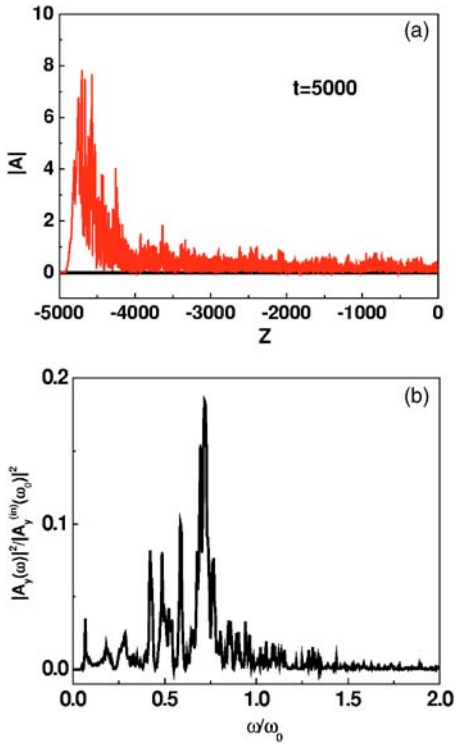

FIG. 16. (a) The profile of reflected field $|\mathbf{A}_\perp|$ at $t=5000$ for the high density case ($\omega_0=0.8$). (b) Normalized spectral intensity of the reflected field.

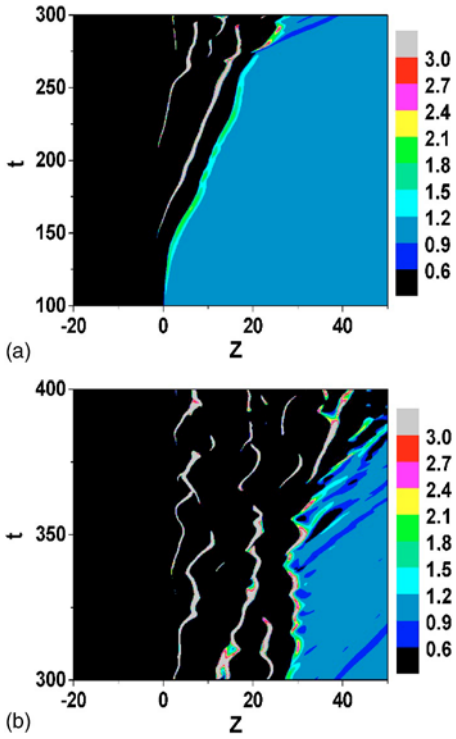

FIG. 17. The nonlinear critical surfaces ($n \geqslant \omega_0^2\gamma$) shown during the time intervals (a) $100<t<300$ and (b) $300<t<400$.

similar effect has been observed in Ref. 35 where PIC simulations were performed for linearly polarized pulses. The mechanism behind the redshifting of the reflected part has been associated with the soliton evolution in an inhomogeneous plasma. We believe that in our case redshifting of the spectrum can be analyzed within the moving-mirror paradigm. In Fig. 17(a) a contour plot of the nonlinear critical surfaces ($n \geqslant \omega_0^2\gamma$) is shown during the time interval in which the leading part of the reflected signal (carrying $\approx$40% of the reflected energy) is formed. The overcritical density layers, developed in the early stages of interaction, move in the direction of the incident pulse propagation with velocities $\beta_c \approx 0.2$. Frequency of the reflected radiation is consequently redshifted, and can be estimated to be $\omega/\omega_0=(1-\beta_c)/(1+\beta_c)\simeq 0.75$.

This frequency corresponds to the largest peak in spectral density of the reflected radiation in Fig. 16(b). Subsequently, the development of new overcritical plasma layers takes place [see Fig. 17(b)]. However, in the next stage of interaction these layers exhibit complex (stochastic) oscillatory motion; it becomes difficult to trace in detail the reflection dynamics of radiation from these layers. What we do observe is that the density drop below the overcritical values [which corresponds to the "breaking" of the bright patterns in Fig. 17(b)] leads to a release of the radiation trapped between the layers. This, in turn, causes the appearance of other peaks (both redshifted and blueshifted) in spectral content of the reflected radiation. Thus, the spectrum of the reflected radiation is considerably broadened. For instance, the spectral peak situated at the left margin in Fig. 16(b) is at $\omega/\omega_0=0.05$ which for $\lambda_0=1$ μm corresponds to a frequency of 15 THz.

In all these simulations, the density in the depleted regions never dropped below $n_{\min}\approx 0.002n_0$. We would like to emphasize that during the entire simulation time, the accuracy of the scheme was controlled by checking the conservation of the integrals of motion. The integrals of motion were conserved with a good precision, making the results perfectly dependable.

It seems obvious that for an overdense plasma layer, the intensive self-induced transparency of the layer can take place if the thickness of the layer is shorter than the distance within which the bulk of the energy resides. Indeed, in Fig. 18 we present the simulation results for just such a finite plasma layer. Keeping all other parameters to be the same as in Fig. 15(b), we choose the layer width to be

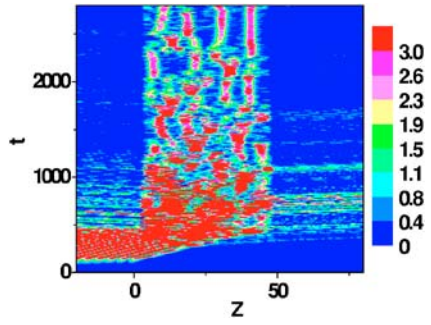

FIG. 18. The t-z diagram of $|\mathbf{A}_\perp|$ for the laser pulse with $A_0=10$, $a_z=126$, and $\omega_0=0.8$ incident on a plasma layer of thickness $L=50$.

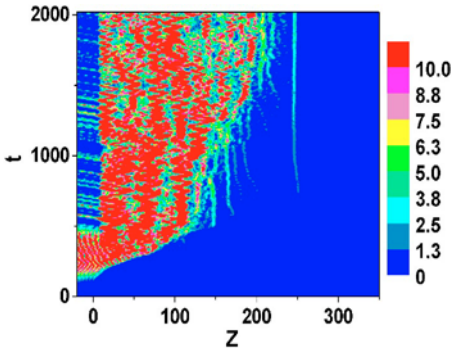

FIG. 19. The t-z diagram of $|\mathbf{A}_\perp|$ for the incident laser pulse with $A_0=10$, $a_z=126$, and $\omega_0=0.8$.

$L=50$—approximately seven times the vacuum wavelength of the laser radiation. In this example, the energy transmitted through the layer is 18% of the incident energy; 80% is reflected, and just 2% of the incident energy still resides in the layer at $t=2800$.

We have conducted a series of simulations for higher pulse intensities. The results come out to be similar to the results for $A_0=5$. This similarity can be seen in Fig. 19 where the field penetration dynamics is shown for $A_0=10$ while all other parameters are kept the same as in Fig. 15(b). We see that the bulk of the penetrated energy still resides near the vacuum-plasma boundary although the penetration region extends all the way to $z\approx 250$. It is also seen that despite its strong spatiotemporal modifications, the plasma electron density does not drop below $n_{\min}\approx 0.0005 n_0$. However, for this large amplitude simulation, the accuracy of the energy integral conservation drops from 1% to 10% for times from $t>2000$ to $t=5000$. To improve the accuracy of the scheme to study the long-time dynamics, the mesh size could be reduced to better resolve the very sharp density gradients.

IV. ELECTRON-POSITRON PAIR PRODUCTION

An interesting byproduct of the interaction of ultrarelativistic laser pulses with a plasma, could be an intensive creation of electron-position (e-p) pairs. It is believed that very high intensity radiation can produce relativistic superthermal electrons. These energetic electrons, interacting with the plasma, can, in turn, generate e-p pairs via bremsstrahlung photons or by colliding with a nucleus (the trident process).[36–39] Naturally for efficient pair production, a significant fraction of the superthermal electrons and the newly produced pairs should be confined and reaccelerated to relativistic energies. In Ref. 36 (see also Ref. 37) it was suggested that this can be realized by using double-sided laser illumination so that the superthermal electrons are confined by the laser ponderomotive pressure in the front and the back and by the strong magnetic fields on the side.

Direct production of e-p pairs is also possible by relativistic electrons driven by the laser field. It was argued in Refs. 40–42 that a laser pulse with intensity larger than $I_{\text{th}}=2\times 10^{19}\lambda_0^{-1}$ W/cm^2 (where the laser wavelength is measured in micrometers) can accelerate the plasma electrons to relativistic speeds with $\gamma\geqslant 3$. These electrons, with kinetic energy in excess of the pair-production threshold $2m_ec^2$, can readily produce e-p pairs by scattering in the Coulomb potential of a nucleus.

There are estimates for the number of e-p pairs created when a laser pulse impinges on either an overdense[41] or an underdense plasma.[42] These estimates, however, are rather rough because the detailed dynamics of laser-plasma interaction is ignored. For instance, the reflected radiation as well as the strong plasma density modifications (in the high field regions) were not taken into account. These effects could severely suppress the number of produced pairs. On the other hand, there could be considerable enhancement in pair production because of the long-time confinement of the relativistic strong radiation in overdense plasma regions.

Neglecting the contribution of the newly created e-p pairs on the overall dynamics, the rate equation governing the pair production (in dimensional form) reads as

$$\frac{\partial n^+}{\partial t}=\sigma_T n n_i v_e, \tag{18}$$

where n^+ is the density of created e-p pairs, $v_e=c(1-\gamma^{-2})^{1/2}$ is the electron velocity, and σ_T is the total cross section of the trident e-p pair production process.[43] Since the pair creation requires the electron relativistic factor $\gamma>3$, it could happen only in regions where the EM field maxima are localized. We remind the reader of the results of the preceding section in which we showed that only a small part of an ultrarelativistic pulse penetrates to a certain depth in an overdense plasma (creating nonstationary field-density structures) while the bulk of the incident energy is reflected from the vacuum-plasma boundary. We also found that in the region of penetration, wherever the field intensity is high, the electron plasma density is reduced considerably due to the action of the ponderomotive force of the EM field. In the relevant region for pair production there are two opposing tendencies at play: the cross section for the trident process increases with γ favoring pair production and the density decrease in the field localization region suppressing the process. The net result will be necessarily detail dependent and to arrive at a believable estimate, we have incorporated Eq. (18) into our numerical scheme; approximate formulas suggested in Ref. 42 (see also Refs. 38 and 39) are used for the cross section of the trident process. For $\gamma<14$ we apply the formula established in Ref. 41,

$$\sigma_T=9.6\times 10^{-4}(Zr_0/137)^2(\gamma-3)^{3.6} \tag{19}$$

while for larger γ, we use the expression[43]

$$\sigma_T=(28/27\pi)(Zr_0/137)^2(\ln\gamma)^3. \tag{20}$$

Here $r_0=2.8\times 10^{-13}$ cm is the classical electron radius and Z is the ion nuclear charge.

We solve Eq. (18) for the field structures created when an ultrarelativistic pulse ($A_0=10$) impinges on a semi-infinite overdense plasma. All parameters of the laser pulse and plasma are the same as shown in Fig. 19. With $\lambda_0=1$ μm, the peak intensity and the duration of the pulse are, respectively,

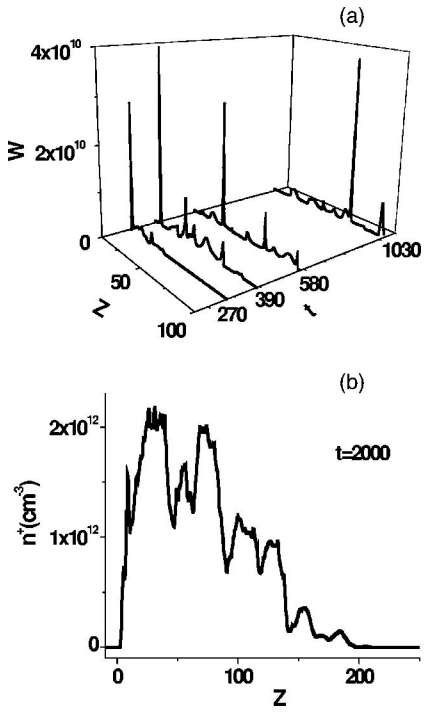

FIG. 20. (a) The pair production rate distribution w in z for different moments of interaction. (b) The pair density n^+ vs z at $t=2000$.

$I \simeq 2.74\times10^{20}$ W/cm^2 and $T_p \simeq 100$ fs. The plasma density is $n_0 \approx 1.8\times10^{21}$ cm^{-3}. In Fig. 20(a) we plot snapshots of the pair production rate $w=\partial n^+/\partial t$ versus z for different t [for convenience the plot is presented in dimensionless units $t \rightarrow \omega_e t$, $z \rightarrow (\omega_e/c)z$]. One can see that the spatiotemporal position of the maxima of the pair production rate are continuously changing in the vicinity $0<z<150$. The pair density at $t=2000$ (which corresponds to 0.9 ps) is shown in Fig. 20(b). The maximum of the e-p pair density is $n^+ \simeq 2\times10^{12}Z^2$ cm^{-3}. The total number of pairs per area $\mathcal{N}^+ = \int n^+ dz$ versus t is given in Fig. 21. One can see that $\mathcal{N}^+ \simeq 2.3\times10^9 Z^2$ pairs are created in 0.9 ps. It is obvious that for larger amplitude pulses and higher density plasmas the number of generated pairs could increase considerably. Here we assumed implicitly that the ions remain at rest for about 1 ps. Simple estimations show that the effects related to the ion motion as well as to the laser field dissipation may reduce the estimated values of the created pairs by no more than a factor of 10.

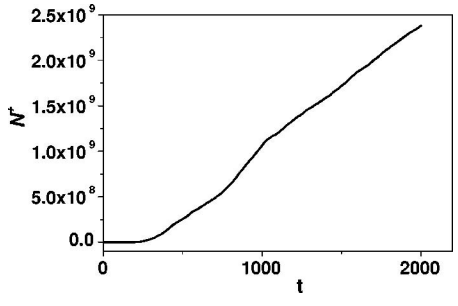

FIG. 21. The accumulated total number of pairs per area $\mathcal{N}^+$ vs t.

Thus, we find that due to the long-time confinement of the relativistically strong radiation near the vacuum plasma boundary, a remarkably large amount of e-p pairs can be generated.

V. CONCLUSION

In this paper we have investigated the interaction of relativistic strong laser pulses with overdense plasmas by numerically solving the full system of Maxwell and collisionless relativistic hydrodynamic equations. It is shown that this approach (accurate dynamical treatment of full set of Maxwell-fluid equations) cannot (and does not) lead to the appearance of zero density anywhere in the plasma. Under certain conditions, the relativistic laser pulse can considerably reduce the electron density in the region of field localization, i.e., the electron cavitation takes place. In the cavitating regions the electron density turns out to be a few orders smaller than its original value, however, the density never becomes strictly zero.

For moderately relativistic pulses, our results from the simulations of exact 1D Maxwell-fluid equations fall in two categories: (1) we confirm qualitatively the results obtained, for instance, in Refs. 13 and 2 we show important quantitative differences as well as expose several essential and interesting features of the interaction. Indeed we do find that for $n_0<1.5n_{cr}$, the moderately intense laser pulses penetrate into the overdense plasma region in the form of solitons while for $n_0>1.5n_{cr}$ the interaction of the laser pulse with semi-infinite electron plasma results in the generation of plasma-field structures consisting of alternating electron and vacuum regions extended into the plasma over a finite length. The details of the soliton formation and parameters of the generated solitons are, however, quite sensitive to initial conditions. These details could lead to totally different scenarios of pulse dynamics interacting with finite plasmas, especially plasmas confined to a thin layer. The generated solitons may not be able to leave such plasma layers; they could be locked in the layer keeping considerable part of the energy of the incident pulse.

For ultrarelativistic pulses it is shown that a major part of the penetrated energy is trapped in a nonstationary plasma layer near the plasma boundary for a long time although solitons could carry a minor part of the energy. This happens regardless of the background density whether it is low ($n_0<1.5n_{cr}$) or high ($n_0>1.5$). The plasma electron distribution consists of a sequence of overcritical density spikes separated by deep density wells where parts of the EM radiation are trapped. The main part of the incident pulse energy (up to 85%) is reflected back from the nonsteady plasma configuration at the vacuum boundary. The reflected signal consists of highly modulated pulses followed by a long train of short subpulses. The spectrum of the reflected field is basically redshifted. Redshifting of the spectrum is explained in terms of the moving-mirror analogy. It is shown that for an overdense plasma layer, the intensive self-induced transparency of the layer can take place only if the thickness of the layer is smaller than the distance where the bulk of the penetrated energy resides in the semi-infinite plasma case.

An additional consequence of the long-time confinement of relativistic strong radiation in overdense plasma region is also analyzed; it is shown that intensive pair production, driven by the motion of plasma electrons, takes place due to the trident process.

We end the paper by pointing out the shortcomings of this effort: In this 1D simulations of full-Maxwell and relativistic hydrodynamic equations of a cold electron plasma, the effects due to ion motion and due to 2D-3D propagation are missing; the missing effects of finite temperature are under investigation.

ACKNOWLEDGMENTS

The authors thank Dr. N. L. Shatashvili for valuable discussions.

The work was supported by ISTC under Grant No. G663. The study of S.M.M. was also supported by the U.S. Department of Energy under Contract No. DE-FG03-96ER-54366.

[1] S. P. Hatchett *et al.*, Phys. Plasmas **7**, 2076 (2000); M. H. Key *et al.*, *ibid.* **5**, 1966 (1998).
[2] D. Umstadter, J. Phys. D **36**, R151 (2003).
[3] P. K. Kaw and J. M. Dawson, Phys. Fluids **13**, 472 (1970).
[4] S. C. Wilks, W. L. Kruer, M. Tabak, and A. B. Langdon, Phys. Rev. Lett. **69**, 1383 (1992).
[5] S. V. Bulanov, N. M. Naumova, and F. Pegoraro, Phys. Plasmas **1**, 745 (1994).
[6] E. Lefebvre and G. Bonnaud, Phys. Rev. Lett. **74**, 2002 (1995); Phys. Rev. E **55**, 1011 (1997).
[7] A. Pukhov and J. Meyer-ter-Vehn, Phys. Rev. Lett. **76**, 3975 (1996).
[8] S. Guerin, P. Mora, J. C. Adam, A. Heron, and G. Laval, Phys. Plasmas **3**, 2693 (1996).
[9] H. Sakagami and K. Mima, Phys. Rev. E **54**, 1870 (1996).
[10] K. Nagashima, Y. Kishimoto, and H. Takuma, Phys. Rev. E **58**, 4937 (1998).
[11] M. Tabak *et al.*, Phys. Plasmas **1**, 1626 (1994).
[12] B. Ritchie and C. D. Decker, Phys. Rev. E **57**, 4645 (1998).
[13] M. Tushentsov, A. Kim, F. Cattani, D. Anderson, and M. Lisak, Phys. Rev. Lett. **87**, 275002 (2001).
[14] V. A. Kozlov, A. G. Litvak, and E. V. Suvorov, Sov. Phys. JETP **49**, 75 (1979).
[15] A. Bourdier and X. Fortin, Phys. Rev. A **20**, 2154 (1979).
[16] V. I. Berezhiani and I. G. Murusidze, Phys. Lett. A **148**, 338 (1990).
[17] B. A. Shadwick, M. Tarkenton, E. H. Esarey, and W. P. Leemans, in *Advanced Accelerator Concepts: Ninth Workshop*, edited by P. L. Colestock and S. Kelley (AIP Conference Proceedings, Vol. 569, pp. 154–162, Santa Fe, New Mexico, 2000).
[18] D. P. Garuchava, Z. I. Rostomashvili, and N. L. Tsintsadze, Fiz. Plazmy **12**, 1341 (1986) [Sov. J. Plasma Phys. **12**, 776 (1986)].
[19] G. Z. Sun *et al.*, Phys. Fluids **30**, 526 (1987); A. B. Borisov *et al.*, Phys. Rev. A **45**, 5830 (1992); X. L. Chen and R. N. Sudan, Phys. Rev. Lett. **70**, 2082 (1993).
[20] F. Cattani, A. Kim, D. Anderson, and M. Lisak, Phys. Rev. E **64**, 016412 (2001).
[21] V. I. Berezhiani, S. M. Mahajan, Z. Yoshida, and M. Pekker, Phys. Rev. E **65**, 046415 (2002).
[22] M. D. Feit *et al.*, Phys. Rev. E **57**, 7122 (1998).
[23] A. B. Borisov *et al.*, Phys. Rev. Lett. **68**, 2309 (1992).
[24] J. H. Marburger and R. F. Tooper, Phys. Rev. Lett. **35**, 1001 (1975).
[25] T. Zh. Esirkepov, F. Kamenets, S. V. Bulanov, and N. M. Naumova, JETP Lett. **68**, 36 (1998).
[26] A. Kim, F. Cattani, D. Anderson, and M. Lisak, JETP Lett. **72**, 241 (2000).
[27] F. Cattani, A. Kim, D. Anderson, and M. Lisak, Phys. Rev. E **62**, 1234 (2000).
[28] E. Esarey, P. Sprangle, J. Krall, and A. Ting, IEEE Trans. Plasma Sci. **24**, 252 (1996).
[29] W. L. Kruer and K. Estabrook, Phys. Fluids **28**, 430 (1985); S. C. Wilks, Phys. Fluids B **5**, 2603 (1993).
[30] L. N. Tsintsadze and K. Nishikawa, Phys. Plasmas **3**, 511 (1996); L. N. Tsintsadze, K. Mima, and K. Nishikawa, Plasma Phys. Controlled Fusion **40**, 1 (1998).
[31] P. K. Kaw, A. Sen, and T. Katsouleas, Phys. Rev. Lett. **68**, 3172 (1992).
[32] V. I. Berezhiani, S. M. Mahajan, and R. Miklaszewski, J. Opt. Soc. Am. B **18**, 617 (2001).
[33] L. V. Hau, S. E. Harris, Z. Dutton, and C. H. Behroozi, Nature (London) **397**, 594 (1999).
[34] V. I. Berezhiani, S. M. Mahajan, and R. Miklaszewski, Phys. Rev. A **59**, 859 (1999).
[35] Y. Sentoku *et al.*, Phys. Rev. Lett. **83**, 3434 (1999).
[36] E. P. Liang, S. C. Wilks, and M. Tabak, Phys. Rev. Lett. **81**, 4887 (1998).
[37] B. Shen and J. Meyer-ter-Vehn, Phys. Rev. E **65**, 016405 (2001).
[38] C. Gahn *et al.*, Phys. Plasmas **9**, 987 (2002).
[39] D. A. Gryaznykh, Y. Z. Kandiev, and V. A. Lykov, JETP Lett. **4**, 257 (1998).
[40] F. V. Bunkin and A. E. Kazakov, Dokl. Akad. Nauk SSSR **193**, 1274 (1970) [Sov. Phys. Dokl. **15**, 758 (1971)].
[41] J. W. Shearer, J. Garrison, J. Wong, and J. E. Swain, Phys. Rev. A **8**, 1582 (1973).
[42] V. I. Berezhiani, D. D. Tskhakaya, and P. K. Shukla, Phys. Rev. A **46**, 6608 (1992).
[43] W. Heitler, *The Quantum Theory of Radiation* (Clarendon, Oxford, 1954).